Coding/Decoding and Reversibility of Droplet Trains in Microfluidic Networks

Michael J. Fuerstman, *et al.*

Science **315**, 828 (2007);
DOI: 10.1126/science.1134514

Science (print ISSN 0036-8075; online ISSN 1095-9203) is published weekly, except the last week in December, by the American Association for the Advancement of Science, 1200 New York Avenue NW, Washington, DC 20005.

15. S. E. Woosley, D. Kasen, S. Blinnikov, E. Sorokina, preprint available at http://arxiv.org/ps/astro-ph/0609562 (2006).
16. P. A. Mazzali, P. Podsiadlowski, *Mon. Not. R. Astron. Soc.* **369**, L19 (2006).
17. P. A. Mazzali *et al.*, *ApJ* **547**, 988 (2001).
18. D. Kasen, S. E. Woosley, preprint available at http://arxiv.org/ps/astro-ph/0609540 (2006).
19. P. A. Mazzali, E. Cappellaro, I. J. Danziger, M. Turatto, S. Benetti, *Astrophys. J.* **499**, L49 (1998).
20. G. Goldhaber *et al.*, *Astrophys. J.* **558**, 359 (2001).
21. W. D. Arnett, *Astrophys. J.* **253**, 785 (1982).
22. A. M. Khokhlov, *Astron. Astrophys.* **245**, 114 (1991).
23. I. Golombek, J. C. Niemeyer, *Astron. Astrophys.* **438**, 611 (2005).
24. S. E. Woosley, S. Wunsch, M. Kuhlen, *Astrophys. J.* **607**, 921 (2004).
25. J. C. Niemeyer, S. E. Woosley, *Astrophys. J.* **475**, 740 (1997).
26. F. K. Roepke, W. Hillebrandt, J. C. Niemeyer, S. E. Woosley, *Astron. Astrophys.* **448**, 1 (2006).
27. D. A. Howell *et al.*, *Nature* **443**, 308 (2006).
28. M. Stritzinger, B. Leibundgut, *Astron. Astrophys.* **431**, 423 (2005).
29. G. Contardo, B. Leibundgut, W. D. Vacca, *Astron. Astrophys.* **359**, 876 (2000).
30. A. W. A. Pauldrach *et al.*, *Astron. Astrophys.* **312**, 525 (1996).

31. We thank E. Pian and D. Sauer for help with data analysis. This work was partly supported by the European Union's Human Potential Programme under contract HPRN-CT-2002-00303, "The Physics of Type Ia Supernovae."

Supporting Online Material

www.sciencemag.org/cgi/content/full/315/5813/825/DC1
Figs. S1 to S5
Table S1
References

12 October 2006; accepted 12 December 2006
10.1126/science.1136259

Coding/Decoding and Reversibility of Droplet Trains in Microfluidic Networks

Michael J. Fuerstman,[1] Piotr Garstecki,[2]* George M. Whitesides[1]*

Droplets of one liquid suspended in a second, immiscible liquid move through a microfluidic device in which a channel splits into two branches that reconnect downstream. The droplets choose a path based on the number of droplets that occupy each branch. The interaction among droplets in the channels results in complex sequences of path selection. The linearity of the flow through the microchannels, however, ensures that the behavior of the system can be reversed. This reversibility makes it possible to encrypt and decrypt signals coded in the intervals between droplets. The encoding/decoding device is a functional microfluidic system that requires droplets to navigate a network in a precise manner without the use of valves, switches, or other means of external control.

The use of microfluidic devices provides a means to study both nonlinear (periodic and chaotic) and reversible behaviors of flows of fluids, although no microfluidic system has simultaneously demonstrated both of these classes of dynamics. At low Reynolds number (Re), the behavior of fluids typically can be reversed—as if the system were going backward in time—by reversing the direction of the forces applied to the system. Recent work has detailed microfluidic systems, which demonstrate nonlinear behaviors such as periodic or chaotic dynamics, that are either inherently irreversible or have not been demonstrated to be reversible (*1*–*3*). Here, we describe a microfluidic device that displays reversible nonlinear dynamics. In this system, droplets of water-based ink moving in hexadecane arrive at a T intersection, where they select one of two paths that form a loop by reconnecting downstream. The binary choices that the droplets make cause the resistance to flow through each branch to evolve in time in a nonlinear fashion: that is, the droplets in each branch influence the choice of subsequent droplets between branches by modifying the rates of flow of liquid through the channels. This behavior results in nonlinear dynamics—droplets select paths with controllable periodicity, and in some instances they choose paths in an aperiodic fashion—whereas the characteristically linear flow of both liquids through the microchannels allows the dynamics to be reversible. We believe that this system can serve as a platform for studying the transition in nonlinear systems from reversible to irreversible dynamics. The reversible, nonlinear dynamics that the device demonstrates are also useful for "lab-on-a-chip" applications—systems that perform physical, chemical, or biological functions on millimeter- to centimeter-scale platforms. For example, we used the device to process a signal represented by sequences of droplets—by encoding and then decoding it—using only the pressure-driven flow of liquids.

Flows at the small length scales (10 to 100 μm) that are characteristic of microfluidic systems typically occur at low Re and thus are dominated by viscosity; inertia plays only a marginal role (*4*). Viscosity-dominated flows are governed by equations of motion that are linear in the velocity of the fluid. Classic experiments by Taylor (*5*) demonstrated how low-Re flows can be reversed. A drop of dye added to a viscous fluid between two cylinders was stretched by rotating the inner one and subsequently reconstituted by reversing the direction of rotation. Recently, Pine *et al*. have investigated a similar system in which colloidal particles in the bulk fluid took the place of the dye in Taylor's experiments (*6*). They demonstrated that the reversibility of the dynamics of the system depended critically on the number of nonlinear events, that is, collisions between particles, that took place during rotation. In both of these systems and in ours, the motion of the carrier fluid can be approximately described by the reversible Stokes equation (*7*).

Microfluidic systems have recently been used to generate multiphase flows where the fluids include suspended droplets (*8*–*10*) and bubbles (*11*–*13*) with substantial control over their size, volume fraction in the carrier fluid, and frequency of production (*14, 15*). The interfacial stresses present in these multiphase systems introduce nonlinearities into the equations of flow, even at low values of Re. These nonlinearities are weak, however, compared with the linear contribution to the dynamics (*16*), and therefore do not affect the reversibility of the movement of bubbles or droplets through a microchannel.

We intentionally introduce an additional, strongly nonlinear component into the interactions that govern the motion of droplets; Fig. 1A shows the device we use. The nonlinearity arises from the binary choice that the droplets make at the T intersection. Each droplet that enters this intersection chooses the branch of the loop through which the hexadecane flows more rapidly—equivalently, the path characterized by the smaller fluidic resistance (*17*). Because the system operates at a capillary number ($<10^{-1}$) that is small enough that the droplets remain intact as they move through the T intersection (*18*), the process of choosing a path amplifies the differences in the rates of flow of hexadecane through the branches of the loop into a binary value; a droplet of aqueous solution is either present in or absent from a branch.

When a droplet moves through a branch of the loop, it increases the resistance to flow in that channel. The droplet consequently decreases the rate of flow of hexadecane through the branch it occupies and increases (at a constant rate of flow) the rate of flow through the other branch (*19*–*21*). Because the next droplet to enter the T intersection also enters the channel through which the hexadecane flows more rapidly, the choice that one droplet makes influences the choice of the next droplet arriving at the junction. This feed-

[1]Department of Chemistry and Chemical Biology, Harvard University, 12 Oxford Street, Cambridge, MA 02138, USA. [2]Institute of Physical Chemistry, Polish Academy of Sciences, Kasprzaka 44/52, 01-224 Warsaw, Poland.

*To whom correspondence should be addressed. E-mail: gwhitesides@gmwgroup.harvard.edu (G.M.W.); garst@ichf.edu.pl (P.G.)

back between successive droplets results in a nonlinear system that exhibits bifurcations and irregular, aperiodic behavior. The nonlinearity in the operation of the system derives from two sources: (i) the time evolution of the fluidic resistances of the two arms of the loop and (ii) the nonlinear transformation of the intervals between droplets entering the loop and those between droplets leaving it. Remarkably, as a result of the precise confinement of the source of the nonlinearity to isolated events, this strongly nonlinear device demonstrates reversibility, a characteristic typical of, but not limited to, linear systems.

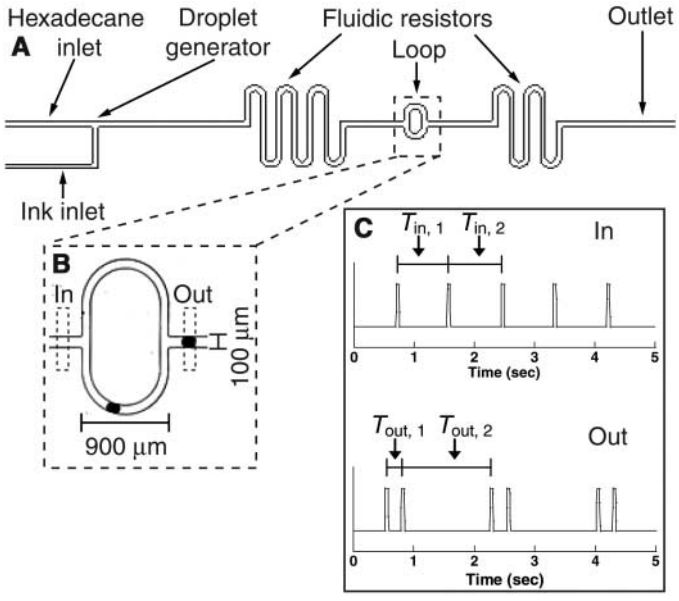

Fig. 1. The microfluidic device. (**A**) A generalized schematic diagram of the microchannel network. Hexadecane containing a surfactant (3% Span-80 by mass) squeezed off droplets of aqueous ink or dye in the T junction. The droplets proceeded to the loop, where they took one of the two paths. (**B**) An optical micrograph of the loop showing one droplet in the lower branch and one droplet in the outlet channel. (**C**) Plots showing the intervals between droplets as they moved through the In and Out windows marked in (B). A spike indicates the presence of a droplet. The upper plot shows uniform time intervals ($T_{in,1}$ and $T_{in,2}$) between droplets as they reached the loop. The lower plot depicts the two different time intervals ($T_{out,1}$ and $T_{out,2}$) that separated droplets as they emerged from the loop when the system operated in period-2 mode.

The basic microfluidic system we use comprises a droplet generator, a section in which a channel branches into a loop and then reconnects, and fluidic resistors (long sections of channel, either folded into a serpentine geometry for compactness or wound into a spiral). Figure 1A sketches the general form of the network. Pressure applied to a reservoir of hexadecane that contains 3% by mass Span 80, a nonionic surfactant, and a reservoir of an aqueous solution of ink or dye, creates droplets at constant intervals of time at a T junction. The droplets then move through a fluidic resistor, which damps the changes in pressure at the T junction caused by droplets navigating through the loop and ensures that the bubbles are produced at a constant frequency. After the resistor, the droplets reach a loop that has asymmetric branches: in the system shown in Fig. 1B, the longer branch is 1.98 mm long and the shorter 1.78 mm. Finally, the droplets travel through another fluidic resistor and out of the system.

We monitored the times at which droplets enter and exit the loop at the positions marked in Fig. 1B using a high-speed charge-coupled-device camera. The behavior of the system depends on the intervals of time that separate the droplets as they arrive at the entrance to the loop. For sufficiently large intervals between drops (t > 1.04 s), only one droplet passes through the loop at a time. As the intervals between droplets decreases to 0.90 s, a droplet arrives at the junction while the previous one still occupies the shorter branch. The increase in the fluidic resistance of the shorter branch due to the presence of the droplet is sufficient to divert every second droplet into the longer branch. Because the rates of flow through each of the branches differ, the intervals between droplets exiting the loops repeat in sequences of a longer interval followed by a shorter one (Fig. 1C); we refer to this regime as "period-2". For 0.90 > t > 1.04 s, the system exhibits period-3 and period-4 behavior.

As we decrease the intervals between droplets entering the loop, the system displays a series of bifurcations to higher-order periodic and aperiodic behaviors. To characterize the periodicities, we construct Poincaré maps, which are plots of the time interval between the nth and n + 1st droplet versus the time interval between the nth and n – 1st droplet (Fig. 2A). The two plots on the left (a and c) correspond to the intervals between droplets before they reach the loop for two different values of the mean interval between droplets (0.679 and 0.591 s for sets i and ii). The right-hand plot (b) in set i depicts the system demonstrating period-3 behavior; the 33 points on this plot fall into three clusters. The right-hand plot in set ii (d) shows the system behaving in an aperiodic manner; the 42 intervals measured do not cluster on the Poincaré map.

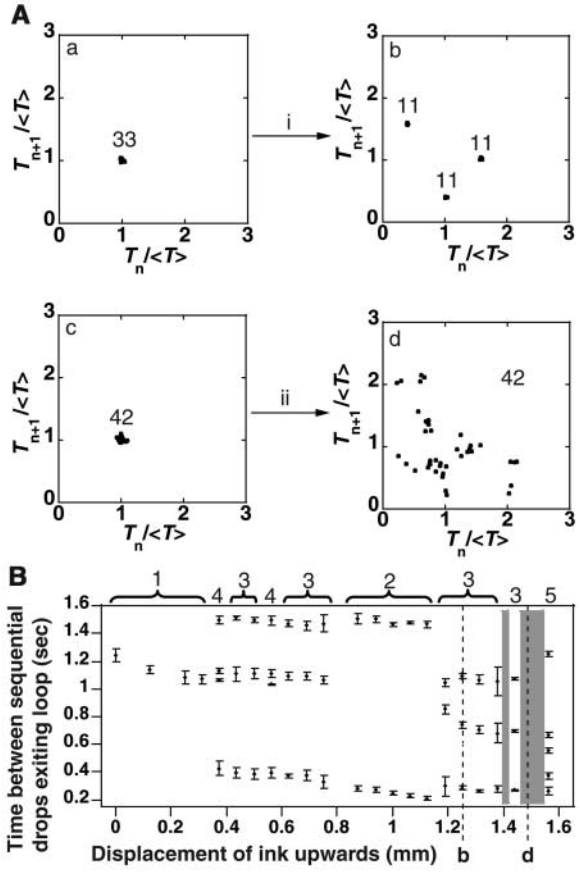

Fig. 2. Periodic and aperiodic behavior. (**A**) Poincaré maps of the system shown in Fig. 1 in (i) period-3 mode and (ii) an aperiodic mode. The maps plot the n + 1st interval (T_{n+1}) versus the nth interval (T_n); the intervals are normalized by the mean of the intervals in each set of data (<T>). The left-hand maps (a and c) show one cluster and indicate that the intervals between drops were uniform as they reached the loop. The number of clusters in map b reveals the trimodal periodicity of the system. Map d shows no discernable clustering and thus denotes aperiodic behavior. The numbers next to the clusters in plots a to c denote the number of data points in each cluster, whereas the number in plot d shows the number of data points in the entire plot. (**B**) A bifurcation diagram for the system. As the displacement (the height of the ink) increased, the periodicity of the system changed. The numbers above the chart denote the periodicity demonstrated for each range of the height of the reservoir of ink. Gray bars denote areas where the system behaved aperiodically. The states of the system as represented by Poincaré maps b and d are marked on the bifurcation diagram.

Figure 2B uses a bifurcation diagram to summarize the periodicities we observe for the one-loop system to the extent that our experimental setup allows us to probe. We fix the pressure of the nitrogen applied to the reservoirs of hexadecane and ink and then raise the vial containing the ink in steps of 250 μm using a micropositioner. Raising this vial increases the pressure applied to the ink due to gravity, increases its rate of flow, and thus decreases the intervals between droplets entering the loop. The resulting periodicities of the paths selected by the droplets change as we vary the pressure applied to the ink. We observe period-1, -2, -3, -4 and -5 behavior, as well as regimes where the droplets select branches aperiodically. The observation of a bifurcation cascade is typical of many nonlinear systems.

To determine whether the dynamics of the system are reversible, we prepare a system containing one loop followed by a spiraling outlet channel ~9.5 cm long (*22*) in which we store the sequence of droplets that exit the loop. We set the pressure applied to the hexadecane and the aqueous solution of dye so that the device operates in period-7 mode for a sufficiently long period of time that the spiral channel fills with droplets in a period-7 configuration. We then reverse the direction of flow through the system by toggling two three-way valves. The valves switch the applied pressure from the hexadecane supply to the outlet of the device (*23*).

Figure 3A shows a time-space diagram of droplets traveling forward and backward through the system. As the system initially evolves in time (before the reversal of the direction of flow), the droplets move from left to right in the channel (the loop is positioned in the center of the plot, accounting for the blank space). We plot the position of each droplet within the channel versus time as the system evolves. The bands on the left side of the plot are evenly spaced, the uniform spacing indicating that the droplets enter the left side of the loop separated by constant intervals of time (the standard deviation of the intervals is 1.2% of the mean interval). The bands on the right side of the time-space plot show that the droplets exit the right side of the loop in intervals that repeat in groups of seven. The Poincaré map on the right in set i of Fig. 3B confirms that the system operates in a period-7 mode while the continuous liquid flows forward through the system. When we reverse the direction of flow through the channels, the droplets enter the right side of the loop in period-7 mode and emerge from the left side in a stream of uniform periodicity. The standard deviation of the intervals increases, however, to 7.5% of the mean time interval after we reversed the direction of flow. The spiral was large enough to hold ~10 periods of seven droplets each. The system demonstrates reversibility over five period-7 groups of droplets but fails to reverse the period-7 behavior to period-1 behavior for longer sequences. We believe that the failure in the reversibility of the system after five periods and the increase in the standard deviation of the intervals are caused by the droplets moving closer together as they are stored in the inner ring of the spiral.

The reversibility of the dynamics of a system depends on the insensitivity of those dynamics to perturbations. The scatter in the right-hand Poincaré map shown in Fig. 3C (ii) demonstrates that the system is subjected to perturbations upon reversal of the direction of flow of hexadecane. Despite these perturbations, the droplets still exit the loop in a period-1 fashion. The dynamics therefore preserve the coherence of the signal.

The device with one loop that we described previously demonstrates reversibility upon reversal of the direction of flow. We found that period-2 sequences, however, are reversible if the droplets are sent forward through a second loop identical to, and downstream of, the first one (Fig. 4, A and B). This property of reversibility without requiring a reversal of the direction of flow is due to backward/forward symmetry. The period-2 sequence ABABAB (where A denotes a longer interval and B a shorter one) looks exactly the same whether read in the forward or reverse direction, with a B always following an A.

We use the two-loop device to encode and decode a signal comprising the intervals of time between droplets. We use the device in Fig. 4A to process an analog signal and the device in Fig. 4B to process a digital one, although both devices are capable of processing either type of signal. To encode the analog signal, we modulate the pressure applied to the reservoir of ink about the

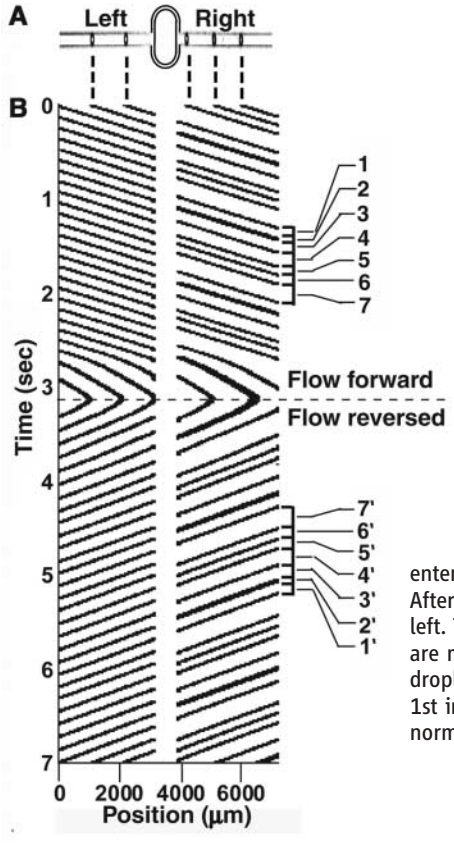

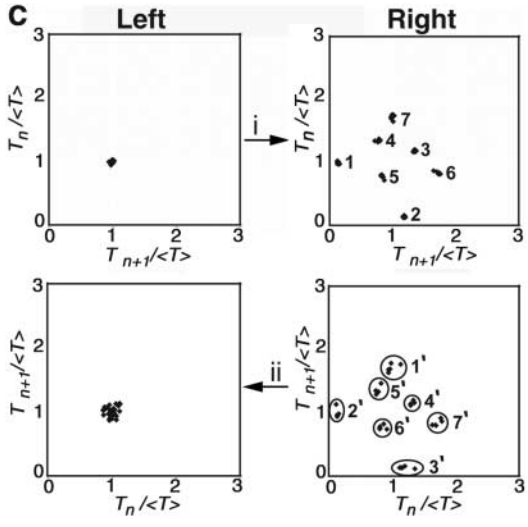

Fig. 3. Reversing the behavior of the system. (**A**) An optical micrograph of droplets moving through the channel on either side of the loop. We stretched the width of the channel relative to its length by a factor of nine, using Adobe Photoshop, to make the droplets more easily visible. The initial positions of the droplets in the optical micrograph correspond to the points at the top of the plot in (B) to which dashed lines are drawn. The loop is drawn schematically and is not part of the optical micrograph. (**B**) A plot of the position of droplets in the system as a function of time. Each horizontal slice of this plot represents a snapshot of the system. The black areas signify the presence of a droplet, and the white parts depict the absence of droplets. The droplets initially move from left to right; they enter the loop with uniform separation and exit separated by a repeating sequence of seven intervals. After the direction of flow of hexadecane through the system is reversed, the droplets move from right to left. They enter the loop in period-7 mode and exit with uniform separation. The seven repeating intervals are marked on the right-hand side of the plot. (**C**) Poincaré maps showing the periodicity of the train of droplets (i) before reversal and (ii) after reversal. The maps in (i) plot the *n*th interval (T_n) versus the *n* + 1st interval (T_{n+1}), whereas the maps in (ii) plot the *n* + 1st versus the *n*th. In all maps, the intervals are normalized by the mean of the intervals in each set of data (<*T*>).

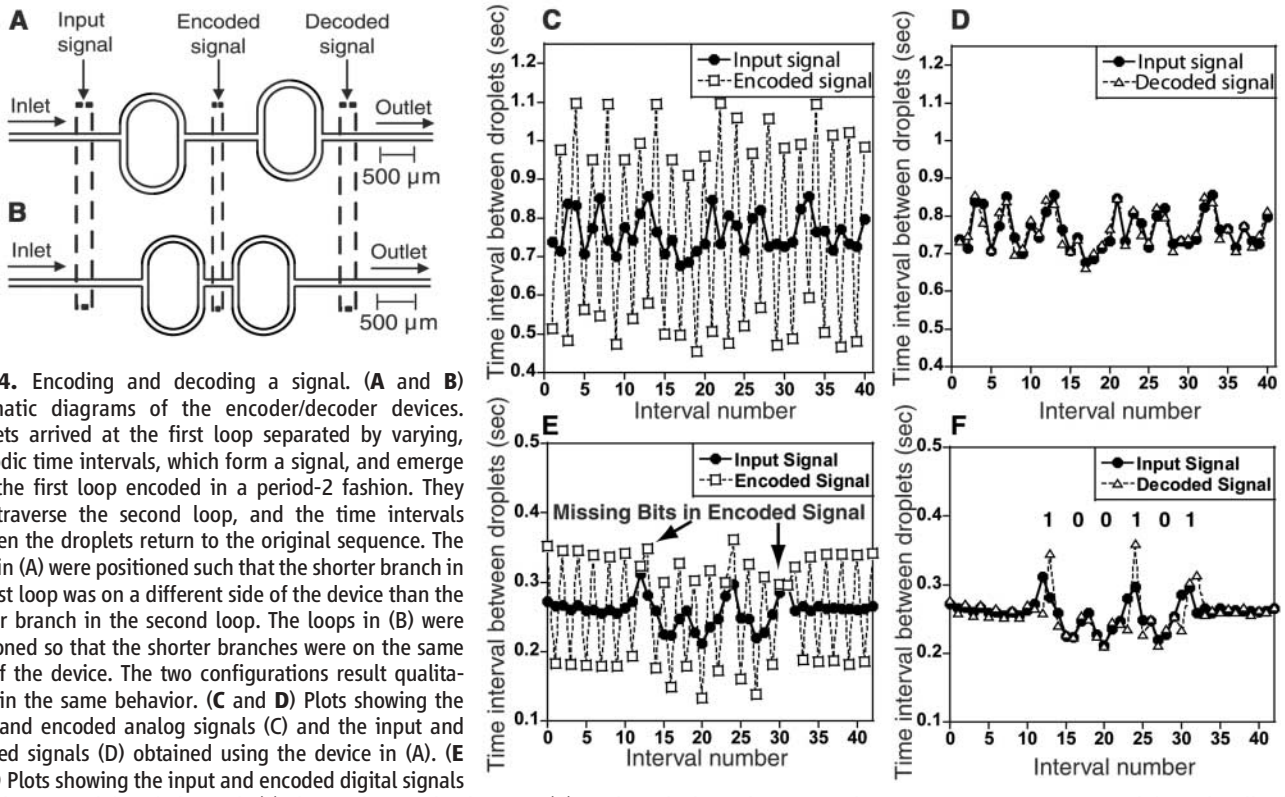

Fig. 4. Encoding and decoding a signal. (**A** and **B**) Schematic diagrams of the encoder/decoder devices. Droplets arrived at the first loop separated by varying, aperiodic time intervals, which form a signal, and emerge from the first loop encoded in a period-2 fashion. They then traverse the second loop, and the time intervals between the droplets return to the original sequence. The loops in (A) were positioned such that the shorter branch in the first loop was on a different side of the device than the shorter branch in the second loop. The loops in (B) were positioned so that the shorter branches were on the same side of the device. The two configurations result qualitatively in the same behavior. (**C** and **D**) Plots showing the input and encoded analog signals (C) and the input and decoded signals (D) obtained using the device in (A). (**E** and **F**) Plots showing the input and encoded digital signals (E) and input and decoded signals (F) obtained using the device in (B). Each peak above the *y*-axis value of 0.280 s represents a 1, while each valley below 0.225 s represents a 0. The digital signal 100101 is equivalent to the decimal number 37. The arrows in (E) show the bits in the input signal that do not appear in the encoded signal but reappear in the decoded signal in (F).

value corresponding to the midpoint of the region characterized by period-2 behavior by adjusting the height of the reservoir of ink between ±1 mm using the micropositioner. Changing the height of the ink in this manner allows for precise control of the pressure applied to the ink. Displacing the reservoir upwards by 0.1 mm results in an increase in pressure of only 0.002 pounds per square inch (psi). The droplets that form while we raise and lower the reservoir of ink are separated by aperiodic intervals of time that range from 0.68 s to 0.86 s. We recorded the time that passes between consecutive droplets moving through the regions marked as "input signal," "encoded signal," and "decoded signal" in Fig. 4A. The first loop encodes the droplets by dramatically changing the sequence of intervals of time between droplets (Fig. 4C). The intervals of the encoded signal differ from the intervals of the input signal by an average of 33.3%. The second loop then decodes the signal (Fig. 4D). The intervals of the decoded signal differ from those that form the input signal by an average of 2.3%.

To encode a digital signal, we use an electronically controlled valve (*23*) to adjust the pressure applied to the reservoir of ink. We set the baseline for the code by applying 1.075 V to the valve (which applies ~3.18 psi of pressure to the reservoir of ink) and 3.26 psi of pressure to the reservoir of hexadecane. The droplets then reach the first loop separated by 0.263 ± 0.005 s. To create a value of 1, we decrease the voltage applied to the valve to 1.074 V to decrease the pressure applied to the ink and increase the intervals between droplets. To express a 0, we conversely increase the voltage applied to the valve to 1.076 V. Figure 4, E and F, shows the input, encoded, and decoded signals for the binary number 100101, which corresponds to the decimal number 37. Two bits in the input signal—the first and last 1's—do not appear in the encoded signal in Fig. 4E. In these two instances, two consecutive droplets (the intervals between which formed the peak of the signals) are separated by sufficiently long periods of time that both droplets choose the same path through the loop. Unexpectedly, the 1's are restored to the signal after the droplets pass through the second loop, although the peaks appear one interval later than in the input signal. This experiment demonstrates that the system can faithfully decode a nontrivially encoded signal.

Pine *et al.* recently studied the boundary between reversibility and irreversibility in the flow of a viscous suspension of colloidal particles. They showed that a critical number of nonlinear collisions between the particles initiates the transition to irreversibility. We used the combination of nonlinear events—the selection of paths by bubbles—and the linear nature of the viscous flow of fluids through microchannels to obtain complex behavior while preserving the reversibility of the system. We used this reversible, nonlinear system to encrypt and decrypt information. The reversible dynamics of the encoder/decoder described in Fig. 4 demonstrate that uncontrolled perturbations do not prevent the manipulation of data coded in trains of droplets. The encoder/decoder is an example of a microfluidic device that generates complex control of trajectories of droplets (e.g., directing drops into predefined branches of microfluidic networks) without using valves or switches.

References and Notes

1. F. Jousse, R. Farr, D. R. Link, M. J. Fuerstman, P. Garstecki, *Phys. Rev. E Stat. Nonlin. Soft Matter Phys.* **74**, 036311 (2006).
2. P. Garstecki, M. J. Fuerstman, G. M. Whitesides, *Phys. Rev. Lett.* **94**, 234502 (2005).
3. P. Garstecki, M. J. Fuerstman, G. M. Whitesides, *Nature Physics* **1**, 168 (2005).
4. H. A. Stone, A. D. Stroock, A. Ajdari, *Annu. Rev. Fluid Mech.* **36**, 381 (2004).
5. G. I. Taylor, in *National Committee for Fluid Mechanics Films* (Education Development Center, Newton, MA, 1966).
6. D. J. Pine, J. P. Gollub, J. F. Brady, A. M. Leshansky, *Nature* **438**, 997 (2005).
7. T. M. Squires, S. R. Quake, *Rev. Mod. Phys.* **77**, 977 (2005).
8. S. L. Anna, N. Bontoux, H. A. Stone, *Appl. Phys. Lett.* **82**, 364 (2003).
9. T. Thorsen, R. W. Roberts, F. H. Arnold, S. R. Quake, *Phys. Rev. Lett.* **86**, 4163 (2001).
10. T. Ward, M. Faivre, M. Abkarian, H. A. Stone, *Electrophoresis* **26**, 3716 (2005).
11. T. Cubaud, C.-M. Ho, *Phys. Fluids* **16**, 4575 (2004).

12. A. M. Ganan-Calvo, J. M. Gordillo, *Phys. Rev. Lett.* **87**, 274501 (2001).
13. P. Garstecki, H. A. Stone, G. M. Whitesides, *Phys. Rev. Lett.* **94**, 164501 (2005).
14. P. Garstecki, M. J. Fuerstman, H. A. Stone, G. M. Whitesides, *Lab Chip* **6**, 437 (2006).
15. P. Guillot, A. Colin, *Phys. Rev. E* **72**, 066301 (2005).
16. F. P. Bretherton, *J. Fluid Mech.* **10**, 166 (1961).
17. W. Engl, M. Roche, A. Colin, P. Panizza, A. Adjari, *Phys. Rev. Lett.* **95**, 208304 (2005).
18. D. R. Link, S. L. Anna, D. A. Weitz, H. A. Stone, *Phys. Rev. Lett.* **92**, 054503 (2004).
19. P. Garstecki, M. A. Fischbach, G. M. Whitesides, *Appl. Phys. Lett.* **86**, 244108 (2005).
20. S. R. Hodges, O. E. Jensen, J. M. Rallison, *J. Fluid Mech.* **501**, 279 (2004).
21. H. Wong, C. J. Radke, S. Morris, *J. Fluid Mech.* **292**, 95 (1995).
22. Fig. S1 details the design of the microfluidic network.
23. Materials and methods are available as supporting material on *Science* Online.
24. This work was supported by the U.S. Department of Energy under award DE-FG02 OOER45852. P.G. thanks the Foundation for Polish Science for financial support. We thank the Harvard Center for Nanoscale Systems for the use of microfabrication facilities and the fast cameras.

Supporting Online Material
www.sciencemag.org/cgi/content/full/1134514/DC1
Materials and Methods
Figs. S1 and S2
References

30 August 2006; accepted 12 December 2006
Published online 4 January 2007;
10.1126/science.1134514
Include this information when citing this paper.

Microfluidic Bubble Logic

Manu Prakash* and Neil Gershenfeld

We demonstrate universal computation in an all-fluidic two-phase microfluidic system. Nonlinearity is introduced into an otherwise linear, reversible, low–Reynolds number flow via bubble-to-bubble hydrodynamic interactions. A bubble traveling in a channel represents a bit, providing us with the capability to simultaneously transport materials and perform logical control operations. We demonstrate bubble logic AND/OR/NOT gates, a toggle flip-flop, a ripple counter, timing restoration, a ring oscillator, and an electro–bubble modulator. These show the nonlinearity, gain, bistability, synchronization, cascadability, feedback, and programmability required for scalable universal computation. With increasing complexity in large-scale microfluidic processors, bubble logic provides an on-chip process control mechanism integrating chemistry and computation.

Microfluidic "lab-on-a-chip" devices, where picoliters of fluids can be precisely manipulated in microscopic channels under controlled reaction conditions, have revolutionized analytical chemistry and biosciences. Recent advances in elastomeric pneumatic microvalves (*1*) and large-scale integration (*2*) have enabled complex process control for a wide variety (*3*, *4*) of applications in single-phase microreactors. However, pneumatic elastomeric microvalves require external macroscopic solenoids for their operation, and cascadability and feedback (where a signal acts on itself) are currently lacking in microfluidic control architectures.

Several reaction chemistries have been implemented in segmented-flow two-phase microreactors, where individual nanoliter droplets traveling inside microchannels are used as reaction containers (*5*, *6*). Dielectrophoretic (*7*) and electrostatic (*8*) schemes have been proposed for on-chip droplet management, but these require external control of individual gates. Devices that exploit the dynamics of droplets inside microchannels would make high-throughput screening and combinatorial studies possible (*9*), but passive techniques (*10*, *11*) have not provided control over individual droplets.

We demonstrate bubble logic that implements universal Boolean logic in physical fluid dynamics. This provides a droplet-level, internal, inherently digital flow control mechanism for microfluidic processors. A bubble traveling in a microchannel can represent a bit of information as well as carry a chemical payload, making it possible to integrate chemistry with computation for process control. Bubble logic preserves the information representation from input to output; thus, devices can be cascaded, allowing implementation of combinatorial and sequential Boolean logic. A bubble can be transported to a desired location in a complex microfluidic network via a series of logic gates corresponding to an equivalent Boolean circuit.

Logic gates have been implemented chemically in chemical concentration waves in a Belousov-Zhabotinsky reaction (*12*) and in DNA (*13*). Purely hydrodynamic fluidic logic (*14*) was used to build a trajectory controller, an all-fluidic display, nondestructive memory, and a simple computer (*15*). Because the high Reynolds numbers required for inertial interactions cannot be maintained in the microscopic geometries needed for higher operating speeds and increasing integration, fluids with non-Newtonian polymer additives have been used to realize a constant flow source and a bistable gate (*16*, *17*). Boolean logic in a single-phase Newtonian fluid was implemented by changes in flow resistance (*18*), but because its input and output representation were not the same, these devices could not be cascaded. Bubble logic, based on hydrodynamic bubble-to-bubble interactions, is more similar in bit representation to theoretical billiard ball logic (*19*) based on the elastic collision of particles, and to magnetic bubble memory (*20*) relying on interactions of magnetic domains in garnet films. These schemes all conserve information, because during a logic operation a bit is neither created nor destroyed.

The pressure-driven flow of bubbles in an interconnected microfluidic network can be described with a simplified dynamic flow resistance model (*21*). Single-phase flow resistance of a channel at low Reynolds number can be approximated as $\Delta p/Q \propto \mu L/h^3 w$, where $\Delta p/LQ$ is defined as the hydraulic resistance per unit length, μ is the dynamic viscosity, and h and w are the height and width of the microchannel. The pressure drop due to a long bubble flowing in a channel, where the bubble radius in an unbounded fluid is greater than the channel width and the continuous phase completely wets the channel surface, is nonlinear and is proportional to $\Delta p \propto \sigma/w(3Ca^{2/3})$, where Ca is the capillary number ($Ca = \mu u/\sigma$), u is the flow velocity of the continuous phase, and σ is the surface tension between liquid and gas phase (*22*, *23*). For small flow rates, this increased flow resistance is primarily due to viscous dissipation in the thin film of liquid surrounding the bubble. With the presence of surfactant molecules on the air-water interface, viscous dissipation in the lubrication film further increases as a result of the no-slip boundary conditions at the interface. In this case, the pressure drop across a finite-length bubble is also linearly dependent on the bubble length until it reaches a critical value, beyond which it is constant (*24*). When a bubble traveling in a microchannel arrives at a bifurcation with low capillary number (where the bubble does not split because surface tension dominates the viscous stress), it chooses the branch with highest instantaneous flow (*25*, *26*).

With an increased flow resistance due to the presence of a bubble in a microchannel, flow lines in surrounding interconnected channels can be perturbed. The nonlinearity in such a system arises from the introduction of interfacial force terms from the boundary conditions due to the presence of a free surface at the fluid interfaces (*27*). These nonlinear time-dependent interactions are the basis of our bubble logic gates. In the implementation described here, we used water as the liquid medium [with added surfactant 2% (w/w) Tween 20 to stabilize the interfaces] and nitrogen bubbles. Planar bubble logic devices were fabricated in poly(dimethyl siloxane) (PDMS) by single-layer soft lithography and plasma bonding to Pyrex substrates.

Center for Bits and Atoms, Massachusetts Institute of Technology, Cambridge, MA 02139, USA.

*To whom correspondence should be addressed. E-mail: manup@mit.edu